Updated Sep. 8th, 2005

Chapter VI. MoM VIE Approach to a Dielectric Material

Contents

6.1. Choice of the basis functions

6.2. MoM edge basis function

6.3. Relation to SWG basis functions

6.4. Size of the functional set

6.5. MoM impedance matrix and MoM equations

6.6. Eigenmode solution

6.7. Modal fields

6.8. Electric/magnetic field and surface charges

6.9. Method of calculation the impedance matrix $\hat{Z}^{DD}$ and the radiated/scattered fields

6.10. List of available Gaussian integration formulas on tetrahedra

6.11. Summary of numerical operations and associated MATLAB/C++ scripts

6.1. Choice of the basis functions

The MoM solution for dielectric objects can be obtained using the method of volume integral equation [1]. This method has a number of advantages including the applicability to inhomogeneous materials [2] and a potentially better accuracy at the resonances (compared to the surface integral formulation [3]). At the same time, it suffers from a rapid growth of computational complexity with increasing grid size. Therefore, possible reduction of the number of basis functions (unknowns) will improve the performance of the method.

The simplest choice is the pulse basis functions (cf. [4]). However, they tend to be unstable when relative permittivity becomes high [1]. The face-based tetrahedral basis functions proposed by Schaubert, Wilton, and Glisson [2] (SWG basis functions) are more robust and are more frequently used today [3, 5]. They enforce the continuity of the normal component of the electric flux density $\vec{D}$ on the faces within the same basis function. This is in contrast to the finite element method with the edge-based basis functions, where the continuity of the tangential $\vec{E}$-field is required on the faces [6-8]. The number of unknowns for the face-based basis functions is equal to the number of the faces of the mesh. For a tetrahedral mesh, the number of faces is considerably greater than the number of the edges. This is a disadvantage compared to the edge-based FEM basis functions, where the number of *independent* unknowns for the system matrix is even smaller than the number of the edges [9, 10].

It is therefore inviting to employ MoM basis functions that still acquire the condition of the continuous normal $\vec{D}$-component according to [2], but include all tetrahedra sharing the edge – similar to the edge-based divergence-free FEM bases [7]. Such basis functions were first introduced by de Carvalho and de Souza Mendes [11].

6.2. MoM edge basis function

The edge-based basis function $\vec{f}$ introduced in [11] is shown in Fig. 6.1. It is similar to the first Whitney form [7]. However, the vector variation is essentially perpendicular to

the base edge $\vec{l}$ (or *AB*). The basis function is defined by a vector of the edge $\vec{p}$ (or *CD*), which is opposite to the base edge $\vec{l}$. Within a tetrahedron, the basis function is a constant field given by $\vec{f} = c\vec{p}$ where *c* is a normalization coefficient.

The basis function may include a different number of tetrahedra that share the same base edge $\vec{l}$. Three representative cases are depicted in Fig. 6.1. In the first case (Fig. 6.1a), both grayed faces of a tetrahedron are on the mesh boundary. The basis function includes only one tetrahedron. In the second case (Fig. 6.1b), two faces of two adjacent tetrahedra are on the mesh boundary. The basis function includes two tetrahedra and has one inner face. In the last case (Fig. 6.1c), all faces of all tetrahedra sharing the base edge are the inner faces of the mesh. The basis function only has the inner faces.

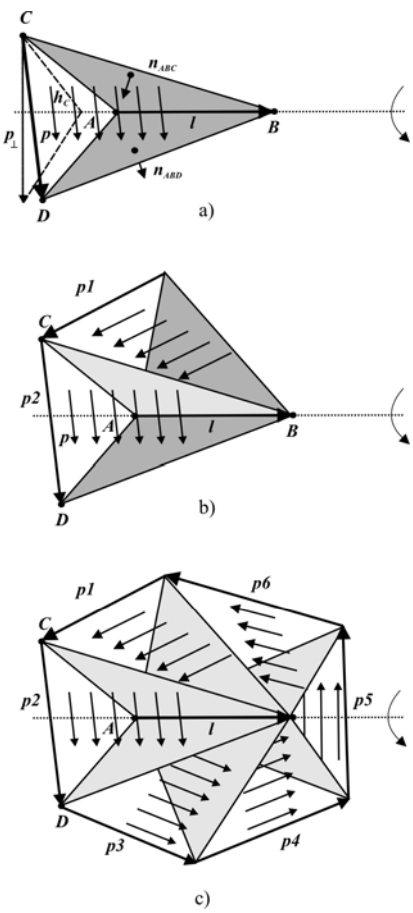

Fig. 6.1. Three possible configurations for the edge-based function: a) – two faces on the mesh boundary and no inner face; b) – two faces on the mesh boundary and one (or more) inner face(s); c) – only inner faces and no boundary faces (Ref. [8] of Introduction © 2004 IEEE).

The component of the basis function $\vec{f}$ normal to face *ABC* in Fig. 6.1a is given by

$$f_{\perp} = c\vec{p} \cdot \vec{n}_{ABC} = c\vec{p}_{\perp} \cdot \vec{n}_{ABC} = 2c\bar{S} / h_C = cl\bar{S} / S_{ABC} \tag{6.1}$$

where $\vec{p}_{\perp}$ is the projection of $\vec{p}$ onto a plane perpendicular to the base edge; h_C is the height of triangle *ABC* perpendicular to the base edge; and $\bar{S}$ is the area of the projection of triangle *ACD* or triangle *BCD* onto a plane perpendicular to the base edge. The normalization coefficient is chosen in the form $c = 1/(l\bar{S})$. This guarantees that (i) the normal component of the basis function is continuous through the inner faces; and (ii) the total flux of the normal component through any face is equal to one.

6.3. Relation to SWG basis functions

It should be noted that edge basis functions can be considered as a subset of the SWG basis functions. Two examples are shown in Fig. 6.2. A piecewise-constant basis function in Fig.2a with four tetrahedra may be expressed as a combination of four SWG basis functions 1-4, shown in Fig. 6.2b. Within tetrahedron ABEF, two linear SWG fields [2] associated with edge AB are combined into a *constant* field parallel to edge AB by a proper choice of one weight constant. Similarly, one edge basis function with two outer faces shown in Fig. 6.2c is represented as a combination of three SWG basis functions 1-3 shown in Fig. 6.2d. Such a linear combination of two SWG basis functions in one tetrahedron eliminates the artificial volume charges [2] from consideration and creates the divergence-free edge basis functions.

6.4. Size of the functional set

A naive guess is to assume that the number of edge basis functions is equal to the number of edges N of the tetrahedral mesh. This approach leads to the ill-conditioned Gram expansion matrix. In order to estimate the number of independent basis functions, let us first consider a mesh with one tetrahedron. Formally, there are six basis functions

corresponding to six basis edges. Only three of them are linearly independent in $\Re^3$ and should therefore be retained. The number of independent basis functions is

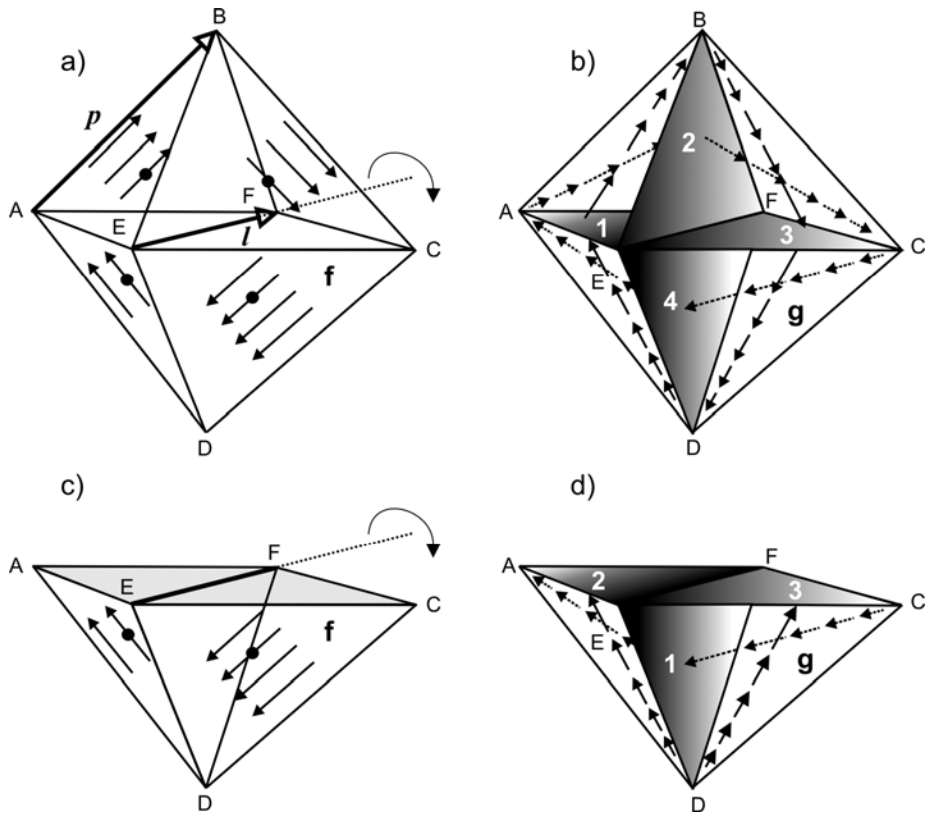

Fig. 6.2. a), c) – Edge basis functions with four/two tetrahedra; b), d) – associated SWG basis functions (grayed facets) for the same configuration of tetrahedra. A piecewise-constant edge basis function in Fig.2a may be expressed as a combination of four SWG basis functions 1-4 shown in Fig. 6.2b (© 2005 IEEE/ACES).

$$N = N_F - N_T \tag{6.2}$$

where N_F is the number of faces (four) and N_T is the number of tetrahedra (one) in the mesh. Next, consider a mesh with two tetrahedra. The component of the electric flux perpendicular to the common face is the same in both tetrahedra, so it is supported by one basis function. The remaining component of the flux (parallel to the face) is different in

both tetrahedra and is supported by two basis functions in each tetrahedron. The number of independent basis functions (five) is again given by equation (6.2) with $N_F = 7, N_T = 2$.

In order to justify equation (6.2) in a general case the following can be mentioned. For any tetrahedral mesh, only one basis function is needed per face to support the normal flux component through the given face. This leads to the first term on the right-hand side of equation (6.2). On the other hand, any tetrahedron has four faces but needs only three linearly independent basis functions. Therefore, one basis function per tetrahedron must be subtracted. This leads to the second term on the right-hand side of equation (6.2). Equation (6.2) was validated directly for a number of uniform and non-uniform meshes of different size and shape. However, a formal proof has not been given.

To remove the dependent basis functions for a given tetrahedral mesh, the Gram or "covariance" matrix of a set of the basis functions on the size $N \times N$ is set in the form

$$G = \begin{bmatrix} \left\langle \vec{f}_1, \vec{f}_1 \right\rangle & \cdots & \left\langle \vec{f}_1, \vec{f}_N \right\rangle \\ \cdots & & \cdots \\ \left\langle \vec{f}_N, \vec{f}_1 \right\rangle & & \left\langle \vec{f}_N, \vec{f}_N \right\rangle \end{bmatrix}, \quad \left\langle \vec{f}_m, \vec{f}_n \right\rangle = \int_V \vec{f}_m \cdot \vec{f}_n d\vec{r} \tag{6.3}$$

The independent columns of matrix G correspond to independent basis functions. Matrix G is reduced by row operations to an echelon form, E, using Gauss-Jordan elimination with partial pivoting [12]. Then, basic columns of matrix E are in the same position as the linearly-independent columns of G [12]. Only these columns are retained. The nullspace of matrix G is eliminated from consideration, similar to the finite elements bases [9].

Since the number of edges in a large tetrahedral mesh is smaller than the number of faces by typically 30 to 40%, the matrix G is smaller than the impedance matrix for the face-based SWG basis functions. Furthermore, it is real and symmetric. Therefore, the elimination of the null space requires approximately 25% of the CPU time required by the factorization of the complex impedance matrix for the face-based basis functions. The critical point is that the elimination of the null space should be done only *once*. When a frequency sweep is applied, the CPU time to eliminate the null space becomes insignificant compared to the total CPU time necessary for the solution of MoM

equations for every frequency. Within the framework of the method of moments, a somewhat similar procedure was described by Rubin [13], who studied certain surface (not volume) basis functions.

6.5. MoM impedance matrix and MoM equations

a. Field and charge expansion

The total electric flux, $\vec{D}(\vec{r})$, has a continuous normal component and is expanded in the form

$$\vec{D}(\vec{r}) = \sum_{n=1}^{N} D_n \vec{f}_n(\vec{r}) \tag{6.3}$$

Once equation (6.3) is applied, the density of the surface bound charges is established following the continuity equation, in terms of the surface δ-functions. The equivalent result can be obtained using Gauss's theorem or the boundary condition on the dielectric-dielectric interface. Consider two arbitrary tetrahedra (plus and minus) that share a common face (which includes the base edge) but have different dielectric constants $\hat{\varepsilon}^{\pm}$. The surface charge density σ_S, from Gauss's law,

$$\sigma_S \equiv (K_+ - K_-)D_\perp = \hat{K}D_\perp \tag{6.4}$$

where K_+ and K_- are the dielectric contrasts of the corresponding tetrahedra and $D_\perp$ is the normal component of the total electric flux density on the boundary. The dielectric contrast $K_\pm = \dfrac{\hat{\varepsilon}^{\pm} - \varepsilon_o}{\hat{\varepsilon}^{\pm}}$ is a constant within every tetrahedron. The dielectric constant $\hat{\varepsilon}^{\pm}$ is a complex number, $\hat{\varepsilon}^{\pm} = \varepsilon'^{\pm}(1 - j\tan\delta)$, for a lossy dielectric. The surface normal is directed from the plus (or left) tetrahedron to the minus (right) tetrahedron.

For every basis function $\vec{f}_n(\vec{r})$, and for every face that supports the normal component of this basis function, the associated surface charge is enforced to follow

equation (6.4). The normal component of $\vec{f}_n(\vec{r})$ can be calculated from equation (6.1). The total surface charge density in the dielectric is obtained from a combination of the contributions of all basis functions

$$\sigma_S(\vec{r}) \equiv \hat{K}(\vec{r})D_\perp(\vec{r}) = \sum_{n=1}^{N}\left\{\sum_{q=1}^{Q}\hat{K}_q f_{\perp nq}(\vec{r})\right\}D_n \quad \vec{r} \in \Omega \tag{6.5}$$

where $\hat{K}_q = K_+ - K_-$ is the differential contrast on face q and $f_{\perp nq}(\vec{r})$ is the normal component of the basis function $\vec{f}_n(\vec{r})$ on face q. The inner summation in equation (6.5) is done over all Q faces that support the normal component of the nth basis function.

The face normal is aligned according to the right-hand rule for the base edge. Its direction follows the direction of the vector field shown in Fig. 6.1. The differential contrast is obtained combining the contrast data for the left and right tetrahedra. If one of them does not exist (vacuum-dielectric boundary), then either K_+ or K_- becomes zero. For a homogeneous dielectric this guarantees that (i) every basis function with only inner faces does not create any surface charges; and (ii) every basis function with two boundary faces possesses zero net surface charge.

Along with (6.5), the volume polarization current density in the dielectric volume, except for any of its boundaries, is given by

$$\vec{J}_V(\vec{r}) \equiv j\omega K(\vec{r})\vec{D}(\vec{r}) = j\omega\sum_{n=1}^{N}\left\{\sum_{p=1}^{P}K_p\vec{f}_{np}(\vec{r})\right\}D_n \quad \vec{r} \in V, \vec{r} \notin \Omega \tag{6.6}$$

The inner summation in equation (6.6) is done over all P tetrahedra that are contained by the nth basis function. Every tetrahedron may possess its own dielectric contrast K_p.

b. MoM equations

According to the volume equivalence principle [1], the piecewise inhomogeneous dielectric material is removed and replaced by equivalent volume polarization currents in

V and by the associated surface bound charges on S. The volume EFIE is written in the mixed-potential form [2]

$$\vec{E}^i = \vec{E} + j\omega\vec{A}(\vec{r}) + \nabla\Phi(\vec{r}) \quad \vec{r} \in V, \vec{r} \in \Omega \tag{6.7}$$

where $\vec{E} = \vec{D}/\hat{\varepsilon}$ is the net electric field and $\vec{E}^i$ is the incident field. The magnetic vector potential $\vec{A}(\vec{r})$ describes radiation of volume polarization currents given by equation (6.6), whereas the electric potential $\Phi(\vec{r})$ describes radiation of the associated bound charges given by equation (6.5). One has

$$\vec{A}(\vec{r}) = \frac{\mu_0}{4\pi}\int_V \vec{J}_V(\vec{r}\,')g(|\vec{r}-\vec{r}\,'|)d\vec{r}\,', \; \Phi(\vec{r}) = \frac{1}{4\pi\varepsilon_0}\int_\Omega \sigma_S(\vec{r}\,')g(|\vec{r}-\vec{r}\,'|)ds' \tag{6.8}$$

where $g = \exp(-jkR)/R, R = |\vec{r}-\vec{r}\,'|$ is the free-space Green's function.

Multiplication of equation (6.7) by $K(\vec{r})\vec{f}_m(\vec{r})$, integration over dielectric volume V, and finally integration by parts of integrals due to $\nabla\Phi(\vec{r})$ for every individual tetrahedron contained by $\vec{f}_m(\vec{r})$ gives N moment equations. The resulting surface integrals must be combined in such a way to extract terms related to differential contrasts $\hat{K}_q$. This gives

$$\begin{aligned}\sum_{p=1}^{P} K_p \int_{V_p} \vec{f}_{mp}(\vec{r})\cdot\vec{E}^i d\vec{r} &= \sum_{p=1}^{P}\frac{K_p}{\hat{\varepsilon}_p}\int_{V_p}\vec{f}_{mp}(\vec{r})\cdot\vec{D}(\vec{r})d\vec{r} + j\omega\sum_{p=1}^{P}K_p\int_{V_p}\vec{f}_{mp}(\vec{r})\cdot\vec{A}d\vec{r} - \\ &\sum_{q=1}^{Q}\hat{K}_q\int_{\Omega_q} f_{\perp mq}(\vec{r})\Phi d\vec{r} \quad m = 1,\ldots,N\end{aligned} \tag{6.9}$$

After substitution of (6.5), (6.6), and (6.8), equation (6.9) gives the MoM equations in the form

$$\upsilon_m = \sum_{n=1}^{N} Z_{mn} D_n \quad \upsilon_m = \sum_{p=1}^{P} K_p \int_{V_p} \vec{f}_{mp}(\vec{r}) \cdot \vec{E}^i(\vec{r}) d\vec{r} \tag{6.10}$$

where the impedance matrix $\hat{Z}^{DD}$ is given by

$$\begin{aligned}
\hat{Z}_{mn}^{DD} &= \sum_{p=1}^{P} \sum_{p'=1}^{P'} \frac{K_p}{\hat{\varepsilon}_p} \int_{V_p} \vec{f}_{mp}(\vec{r}) \cdot \vec{f}_{np'}(\vec{r}) d\vec{r} \\
&- \frac{\omega^2 \mu_0}{4\pi} \sum_{p=1}^{P} \sum_{p'=1}^{P'} K_p K_{p'} \int_{V_p} \int_{V_{p'}} g(|\vec{r} - \vec{r}'|) \vec{f}_{mp}(\vec{r}) \cdot \vec{f}_{np'}(\vec{r}') d\vec{r} d\vec{r}' \\
&- \frac{1}{4\pi\varepsilon_0} \sum_{q=1}^{Q} \sum_{q'=1}^{Q'} \hat{K}_q \hat{K}_{q'} \int_{\Omega_q} \int_{\Omega_{q'}} g(|\vec{r} - \vec{r}'|) f_{\perp mq}(\vec{r}) f_{\perp nq'}(\vec{r}') ds ds' \qquad m, n = 1, \ldots, N
\end{aligned} \tag{6.11}$$

The symmetric impedance matrix is thus written as a combination of individual volume and surface integrals. Since both the basis/test functions and their normal components are constant for a given tetrahedron/face, equation (6.11) may be notably simplified. In terms of the notations of subsection 6.2 one has

$$\begin{aligned}
\hat{Z}_{mn}^{DD} &= \sum_{p=1}^{P} \sum_{p'=1}^{P'} \frac{K_p V_p}{\hat{\varepsilon}_p l_m l_n \bar{S}_{mp} \bar{S}_{np'}} \left(\vec{p}_{mp} \cdot \vec{p}_{np'}\right) \delta_{pp'} \\
&- \frac{\omega^2 \mu_0}{4\pi} \sum_{p=1}^{P} \sum_{p'=1}^{P'} \frac{K_p K_{p'}}{l_m l_n \bar{S}_{mp} \bar{S}_{np'}} \left(\vec{p}_{mp} \cdot \vec{p}_{np'}\right) \int_{V_p} \int_{V_{p'}} g(|\vec{r} - \vec{r}'|) d\vec{r} d\vec{r}' \\
&- \frac{1}{4\pi\varepsilon_0} \sum_{q=1}^{Q} \sum_{q'=1}^{Q'} \frac{\hat{K}_q \hat{K}_{q'}}{S_q S_{q'}} \int_{\Omega_q} \int_{\Omega_{q'}} g(|\vec{r} - \vec{r}'|) ds ds' \qquad m, n = 1, \ldots, N
\end{aligned} \tag{6.12}$$

Note that the first term on the right-hand side of equation (6.12) is only different from zero when the p-th tetrahedron of basis function *m* coincides with the p'-th tetrahedron of basis function *n*.

6.6. Eigenmode solution

a. Preconditioner

A simplest diagonal preconditioner preserving the matrix symmetry [14]

$$\hat{Z}^{DD} \rightarrow L^{-1}\hat{Z}^{DD}L^{-1} \tag{6.13a}$$

is applied to the impedance matrix, where L^{-1} is a real diagonal matrix with the elements

$$l_{mm} = 1/\sqrt{\left|\hat{Z}^{DD}_{mn}\right|} \tag{6.13b}$$

b. Eigenmode solution

The eigenmode solution is then obtained by the search for the local minimum of a cost function F of two variables – the reciprocal condition number κ of the symmetric complex indefinite impedance matrix

$$F(f, f') = \frac{1}{\kappa(\hat{Z}^{DD})} = \frac{1}{\left\|\hat{Z}^{DD}\right\| \cdot \left\|\hat{Z}^{DD^{-1}}\right\|} \tag{6.14}$$

Here, f is the real part of frequency on a complex search plane $f + jf'$ and $f' > 0$ is the imaginary part. If the complex angular frequency is given by $\sigma + j\omega$ [15, 16], then $f' = -\sigma/(2\pi)$.

The `LAPACK` condition estimator implemented in `Intel® Math Kernel Library` is used, based on `zsycon`, which in its turn uses Bunch-Kaufman LU factorization routine `zsytrf` for a symmetric complex matrix [17]. Additionally, it uses `zlansy` to estimate the 1-norm of the impedance matrix [17]. Typical non-resonant conditioning numbers are on the order of $10^4 - 10^7$. The search procedure implies direct evaluation of the cost function on the plane of complex frequency. The resonant frequency and the quality factor of the resonator are then obtained as (cf., for example, [18])

$$f_{res} = f_{\min}, Q = \frac{f_{\min}}{2 f'_{\min}} \tag{6.15}$$

The Q-factor in Eq. (6.15) takes into account not only the losses in the non-ideal (lossy) dielectric but also the radiation loss into free space. The latter usually dominates for an unshielded resonator. Note that in Ref. [16] the Q-factor obtained for these conditions is called the *radiation* Q-factor.

The direct search procedure used in the present version of the program is time-consuming but reasonably safe, especially for closely spaced resonances.

6.7. Modal fields

For a reliable mode identification, it is necessary to compute the detailed field distribution in the resonator [15]. The modal fields are determined using the method described in Ref. [15]. The value of one D-coefficient is chosen to be a constant, corresponding to the electric field $E = 1e-3\,V/m$ in vacuum, namely

$$D_1 = 0.001 \times \varepsilon_0 \tag{6.16}$$

Then , the first row and the first column of the impedance matrix are removed. The resulting truncated impedance matrix $\hat{Z}'$ is used to determine the rest of the coefficients $\vec{D}'$, which satisfy the following (presumably non-singular) system of equations

$$\hat{Z}' \cdot \vec{D}' = \vec{\upsilon}'; \quad \vec{D}' = [D_2, ..., D_N]; \quad \vec{\upsilon}' = -[Z_{21} D_1, ..., Z_{N1} D_1] \tag{6.17}$$

Eqs. (6.17) are solved using the LAPACK matrix solver `zsysv` with diagonal pivoting for complex symmetric matrices [17].

In some cases, assigning a fixed value to D_1 does not lead to an accurate field description, which means that the resulting Eqs. (6.17) are still close to singular ones.

One reason may be the appearance of two (or even more) different resonant modes, at approximately the same frequency. This corresponds to double eigenvalue $\lambda = 0$ and null space of Z of rank 2. Another reason may be numerical inaccuracy due to large variations of the modal fields.

What if the solution is not satisfactory, i.e. $|D_1|$ appears to be much larger than the magnitude of other D-coefficients obtained using Eqs. (6.17)? In this case one may choose another coefficient $D_{n\neq 1}$ in Eq. (6.16) that is the closest one to the average value of D-coefficients, and repeat the solution of Eqs. (6.17). Though slow, this method shows reliable results for different resonator types and modal fields, and it has been implemented in the present program (script `mode.m`).

6.8. Electric/magnetic field and surface charges

Once all D-coefficients are known, one (direct) method to find the electric field within the dielectric is to use the relation

$$\vec{E} = \vec{D} / \hat{\varepsilon} \tag{6.18}$$

and Eq. (6.3). Yet it would be difficult to find the magnetic field with this approach. The density of the surface bound charges is obtained according to Eq. (6.5).

The standard method for field evaluation, implemented in the program, is based on the use of the potential integrals Eqs. (6.8). According to Eqs. (6.7), (6.8), the scattered electric field $\vec{E}^s$ due to volume polarization currents and surface bound charges caused by the electric flux density $\vec{D}$ has the form

$$\begin{aligned}\vec{E}^s(\vec{r}) = {} & \frac{\omega^2 \mu_0}{4\pi} \sum_{n=1}^{N} \left\{ \sum_{p=1}^{P} K_p \int_{V_p} g(|\vec{r} - \vec{r}\,'|)\, \vec{f}_{np}(\vec{r}\,')\, d\vec{r}\,' \right\} D_n \\ & - \frac{1}{4\pi\varepsilon_0} \sum_{n=1}^{N} \left\{ \sum_{q=1}^{Q} \hat{K}_q \int_{\Omega_q} \nabla_r g(|\vec{r} - \vec{r}\,'|)\, f_{\perp nq}(\vec{r}\,')\, ds' \right\} D_n\end{aligned} \tag{6.19}$$

Similarly, the scattered magnetic field $\vec{H}^s$ has the form

$$\vec{H}^s(\vec{r}\,') = -\frac{j\omega}{4\pi}\sum_{n=1}^{N}\left\{\sum_{p=1}^{P} K_p \int_{V_p}\left(\vec{f}_{np}(\vec{r}\,')\times\nabla_r g(|\vec{r}-\vec{r}\,'|)\right)d\vec{r}\,'\right\}D_n \tag{6.20}$$

All the notations in Eqs. (6.19) and (6.20) are identical to those used in Eqs. (6.11) and (6.12) for the impedance matrix.

Once both the electric and magnetic fields are calculated, the Poynting vector $\vec{P}$ within the dielectric material can be found in the form

$$\vec{P} = \frac{1}{2}[\vec{E}\times\vec{H}^*] \tag{6.21}$$

6.9. Method of calculation the impedance matrix $\hat{Z}^{DD}$ and the radiated/scattered fields

a. Base integrals

About 90% of the CPU time required for the filling of the MoM impedance matrix $\hat{Z}^{DD}$ for the edge basis functions is spent for the calculation of the volume/surface integrals presented in Eq. (6.12)

$$A_{D\,pp'} = \int_{V_p}\int_{V_{p'}} g(|\vec{r}-\vec{r}\,'|)d\vec{r}\,d\vec{r}\,' \tag{6.22}$$

$$\Phi_{D\,qq'} = \int_{\Omega_q}\int_{\Omega_{q'}} g(|\vec{r}-\vec{r}\,'|)d\Omega' d\Omega \tag{6.23}$$

In contrast to the metal surface (cf. Chapter 5), no vector integrals are present in the impedance matrix. Also, there are no mixed surface-to-volume integrals.

b. Singularity extraction

The singularity of the free-space Green's function is integrable in 3D or 2D but the accuracy of the Gaussian formulas is reduced if this singularity is retained. Therefore, singularity extraction may be used in Eqs. (6.22), (6.23), in the form

$$\int_{V_p}\int_{V_{p'}} g(|\vec{r}-\vec{r}'|)d\vec{r}d\vec{r}' = \int_{V_p}\int_{V_q} \frac{1}{|\vec{r}-\vec{r}'|}d\vec{r}d\vec{r}' + \int_{V_p}\int_{V_q} \frac{\left(\exp(-jk|\vec{r}-\vec{r}'|)-1\right)}{|\vec{r}-\vec{r}'|}d\vec{r}d\vec{r}' \tag{6.24}$$

$$\int_{\Omega_q}\int_{\Omega_{q'}} g(|\vec{r}-\vec{r}'|)d\Omega' d\Omega = \int_{\Omega_p}\int_{\Omega_q} \frac{1}{|\vec{r}-\vec{r}'|}d\Omega' d\Omega + \int_{s_p}\int_{s_q} \frac{\left(\exp(-jk|\vec{r}-\vec{r}'|)-1\right)}{|\vec{r}-\vec{r}'|}d\Omega' d\Omega \tag{6.25}$$

Two first singular integrals on the right-hand side of Eqs. (6.24), (6.25) (the potential or static integrals) may be found with the help of the analytical results given in [19].

c. Impedance matrix

A "neighboring" sphere of dimensionless radius R is introduced for every integration tetrahedron/facet. R a threshold value for the ratio distance/size. The size of the facet $S(\Omega_q)$, is measured as the distance from its center to the furthest vertex – see Section 5.5 of Chapter V. The size of the tetrahedron $S(V_q)$ is measured exactly in the same way. The observation face Ω_q lies within the sphere if the following inequality is valid for the distance d between two triangle centers

$$\frac{d}{\sqrt{S(\Omega_q)S(\Omega_{q'})}} < R \tag{6.26}$$

If a pair of facets satisfies Eq. (6.26) then the integrals (6.23) use the singularity extraction (6.25) and the analytical formula (5.23) of Chapter V for the inner potential integrals. The non-singular part and the outer potential integrals employ Gaussian cubatures given in [20]. Each cubature is characterized by two numbers: N-the number of integration points; and d-the degree of accuracy for the Gaussian cubature formula. If a pair of facets does not satisfy Eq. (6.26) then the central-point approximation is used for

all integrals, without singularity extraction. The parameter R is initialized in the script `dielectric.m` in subfolder `2_basis\codes`. The same is valid for N and d for the Gaussian formulas. The default values are $R=\sqrt{5}$ and $N=3, d=2$ for the surface integrals. These values are identical with the metal integration values given in Chapter V.

For tetrahedra, the same condition has to be satisfied, in the form

$$\frac{d}{\sqrt{S(V_p)S(V_{p'})}} < R \tag{6.27}$$

If a pair of tetrahedra satisfies Eq. (6.27) then the integrals (6.22) use the singularity extraction (6.24) and the following analytical formula [19]

$$\int_{V_{p'}} \frac{1}{|\vec{r}-\vec{r}'|}\, d\vec{r}' =$$
$$\frac{1}{2}\sum_{j=1}^{4} d_j \left\{ \sum_{i=1}^{3} \vec{\mathrm{P}}_{ij}^{0} \cdot \vec{u}_{ij} \left[|\, d_j \,| \left(\tan^{-1} \frac{\mathrm{P}_{ij}^{0}\, l_{ij}^{+}}{\left(R_{ij}^{0}\right)^2 + |\, d_j \,| R_{ij}^{+}} - \tan^{-1} \frac{\mathrm{P}_{ij}^{0}\, l_{ij}^{-}}{\left(R_{ij}^{0}\right)^2 + |\, d_j \,| R_{ij}^{-}} \right) - \mathrm{P}_{ij}^{0} \ln \frac{R_{ij}^{+} + l_{ij}^{+}}{R_{ij}^{-} + l_{ij}^{-}} \right] \right\} \tag{6.28}$$

for the inner potential integrals. The variables in Eq. (6.28) are similar to those used in Eqs. (5.23) and (5.24) of Chapter V. Here, the double subscript ij represents the ith edge of the jth face of a tetrahedron V. The non-singular part and the outer potential integrals employ Gaussian cubatures on tetrahedra given in [20]. Each cubature is also characterized by two numbers: N-the number of integration points; and d-the degree of accuracy for the Gaussian cubature formula. If a pair of tetrahedra does not satisfy Eq. (6.27) then the central-point approximation is used for all integrals, without singularity extraction. The parameter R is initialized in the script `dielectric.m` in subfolder `2_basis\codes`. The same is valid for N and d for the Gaussian formulas. The default values are $R=1e-3$ and $N=1, d=1$ for the volume integrals. They mean the lowest possible integration accuracy where only the double self-integrals use the singularity extraction Eq. (6.24) and the central-point approximation otherwise. The direct

validation of this approximation is given in Refs. [21, 22] and is connected to the structure of the basis functions themselves. Intuitively, the higher is the integration accuracy, the better the intrinsic "inaccuracy" of the basis functions is reproduced. This inaccuracy implies piecewise-constant field approximation and discontinuity of the tangential *E*-field on the faces. Therefore, the convergence is slow for finer integration. On the other hand, the central-point approximation leaves function behavior on faces essentially undefined. In other words, the existing MoM equations become equally valid for a better (or higher-order) set of basis functions that preserve field continuity. Hence the convergence considerably improves. The more formal discussion with regard to the numerical integration accuracy is given in Chapter VIII.

c. Test of volume/surface potential integrals

The accuracy of the numerical implementation of Eq. (5.23) and Eq. (6.28) has been extensively tested. As an example, Fig. 6.3 shows the integral behavior (absolute integral value) for two equal faces (Fig. 6.3a) and tetrahedra (Fig. 6.3c) separated by a varying distance *s*. Fig. 6.3b gives the potential integral from Eq. (6.25) for $N = 1, d = 1$ (curve 1), $N = 7, d = 5$ (curve 2), and $N = 25, d = 10$ (curve 3). N and d are related to the Gaussian cubature applied to the outer potential integral in Eq. (6.25). Relative error vs. the result of direct integration with 256×256 barycentric points is given by curves $1'$, $2'$, $3'$. To obtain the error percentage, the relative error should be multiplied by 100. Similarly, Fig. 6.3d gives the potential integral from Eq. (6.24) found for $N = 1, d = 1$ (curve 1), $N = 5, d = 3$ (curve 2), and $N = 15, d = 5$ (curve 3) – all these numbers are related to the outer integral. Relative error vs. the result of direct integration with 512×512 barycentric points is given by curves $1'$, $2'$, $3'$. Fig. 6.3e presents the magnified relative error for $N = 5, d = 3$ (curve $2'$), $N = 15, d = 5$ (curve $3'$), and $N = 33, d = 7$ (curve $4'$). These results confirm the accuracy of the potential integrals and, simultaneously, highlight the effect of the outer Gaussian integration. A similar test was made for the vector potential integrals of Chapter V.

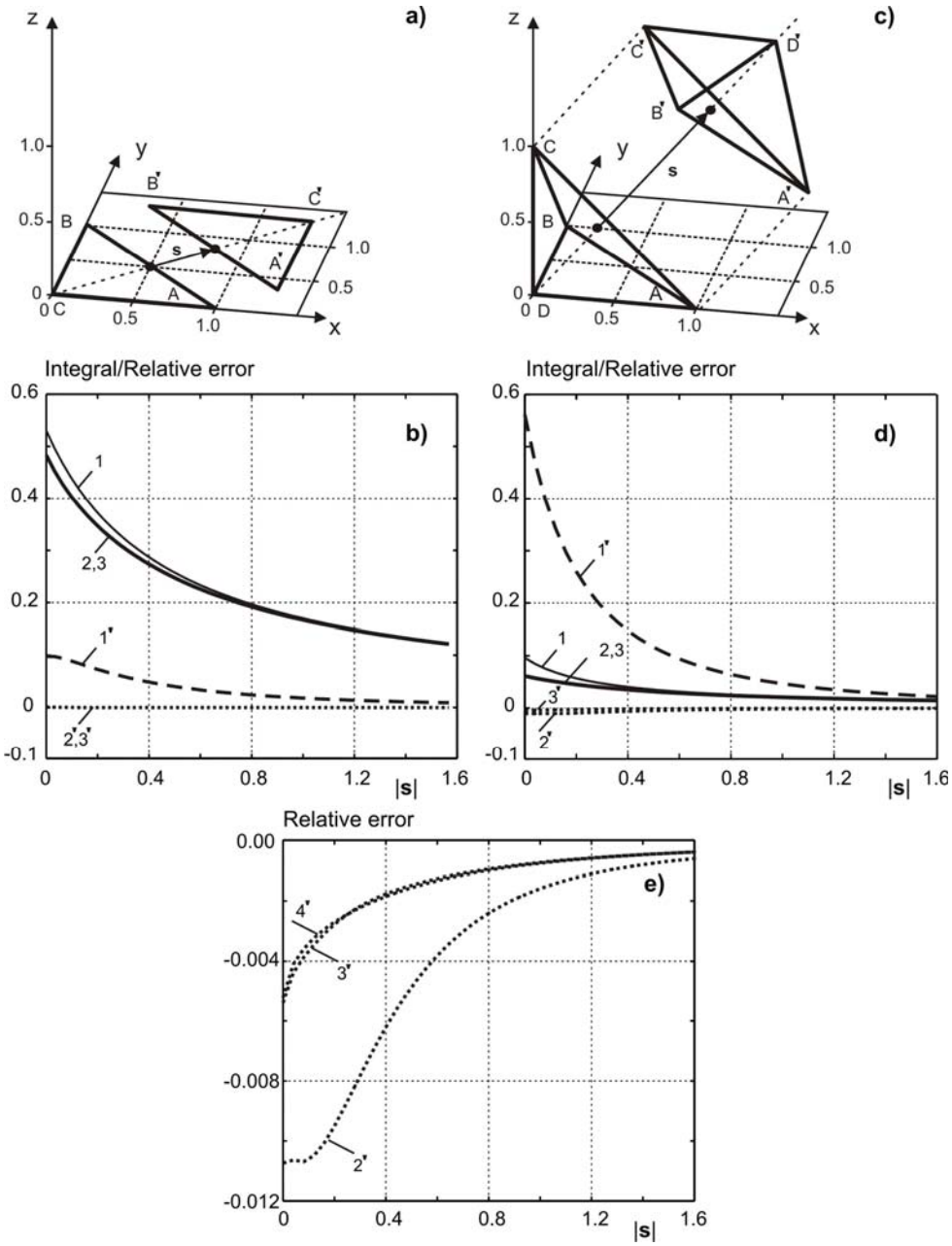

Fig. 6.3. a) – Pair of faces used to evaluate the surface double potential integral; b) – potential integral found for $N=1, d=1$ (curve 1), $N=7, d=5$ (curve 2), and $N=25, d=10$ (curve 3). Relative error vs. the direct solution with 256×256 barycentric points is given by curves $1'$, $2'$, $3'$. c) – Pair of tetrahedra used to evaluate the volume double potential integral; d) –volume potential integral found for $N=1, d=1$ (curve 1), $N=5, d=3$ (curve 2), and $N=15, d=5$ (curve 3). Relative error vs. the direct solution with 512×512 barycentric points is given by curves $1'$, $2'$, $3'$. e) – Magnified relative error for $N=5, d=3$ (curve $2'$), $N=15, d=5$ (curve $3'$), and $N=33, d=7$ (curve $4'$).

d. Fields

The same operation as for the impedance matrix is done for the field integrals (6.19) and (6.20) but Eq. (6.26) is now replaced by

$$\frac{d}{S(\Omega_q)} < R \tag{6.29}$$

Eq. (6.27) changes accordingly. Within the sphere, all the surface potential integrals are found identical to these for the metal structure in Chapter V, with the use of Eqs. (5.23), (5.24), and (5.29) of Chapter V. The volume potential integrals are found according to Eq. (6.28). Additionally, the divergence theorem is used for the potential integrals of the Green's function gradient over tetrahedra, i.e.

$$\int_{V_p} \nabla \frac{1}{|\vec{r}-\vec{r}'|}\, d\vec{r}' = \int_S \frac{1}{|\vec{r}-\vec{r}'|}\, \vec{n}\, ds \tag{6.30}$$

where $\vec{n}$ is the unit outer normal vector to the to each of the four triangular surfaces of the tetrahedron.

The parameter R is initialized in the script `field.m` in subfolder `3_mom/codes`. The default value is $R = 2$. The N and d for the Gaussian formula on facets are hard programmed as $N = 7, d = 5$ in the script `fieldd.cpp`. Similarly, the N and d for the Gaussian formula on tetrahedra are hard programmed as $N = 5, d = 3$ in the same script Outside the sphere, the central-point approximation is used. For the far-field approximation, $R \to 0$ is an acceptable assumption.

6.10. List of available Gaussian integration formulas on tetrahedra

Some Gaussian integration formulas on tetrahedra [20] are given in the script `tet.m` in subfolder `2_basis\codes.` The formulas given in Table 6.1 were used and tested. Each

cubature is characterized by two numbers: N is the number of integration points and d is the degree of accuracy for the Gaussian cubature formula.

Table 6.1. List of available/tested Gaussian formulas on tetrahedra [20].

Formula	N	d
#1	1	1
#2	4	2
#3	5	3
#4	11	4
#5	14	5
#6	15	5
#7	33	7
#8	53	9

Also, the barycentric tetrahedron subdivision of a low degree is available in the script `tet.m`.

6.11. Summary of numerical operations and associated MATLAB/C++ scripts

The summary of numerical operations related to a dielectric resonator is given in Table. 6.2.

Table 6.2. Resonator-related numerical operations.

Resonator operations			
Operation	Script	Path	Remarks
Determine the dielectric structure	`struct2d.m` `struct3d.m`	`1_mesh`	Do not use $\varepsilon_r = 1$ while running `struct3d.m`. Remove all unnecessary tetrahedra from the mesh.
Determine parameters of the edge basis functions and the independent basis function set	`wrapper.m`	`2_basis`	Outputs structure `GEOM` with all the necessary data on the basis functions/precalculated potential integrals
Determine accuracy of impedance matrix filling –optional (see Section 6.9)	`dielectric.m`	`2_basis\codes`	The parameter R is initialized in the script `dielectric.m` in subfolder `2_basis\codes`. The same is valid for N and d for the Gaussian formulas (facets, tets). The default values are $R = \sqrt{5}$ and

			$N=3, d=2$ for the facets and $R=1e-3$ and $N=1, d=1$ for tetrahedra. The necessary potential integrals are pre-calculated in structure `GEOM` and are saved in the sparse matrix format.
Determine eigenfrequency/Q-factor	`eigenfreq.m`	`3_mom`	Fully interactive interface.
Determine the eigenmode field	`mode.m`	`3_mom`	Follows Section 6.7 of this Chapter. Does not work for the metal-dielectric structure. Use `scatterfield.m` instead
Determine the electric or magnetic field distribution in the dielectric volume (or bound surface charge density) in the resonant mode	`scatterfield.m`	`3_mom`	Should be run after `eigenfreq.m`. `Scatterfield.m` illiminates the resonator by an incident plane wave at the resonant frequency and finds the current/charge distributions at that given frequency

If the modal fields obtained after running `mode.m` are not quite well developed, the search domain in `eigenfreq.m` must be refined. The independent scattering problem may be also considered for the dielectric, by running `scatterfield.m` at a given frequency.

References

1. A. F. Peterson, S. L. Ray, and R. Mittra, *Computational Methods for Electromagnetics*, IEEE Press, Piscataway, New Jersey, 1998.
2. D. H. Schaubert, D. R. Wilton, and A. W. Glisson, "A tetrahedral modeling method for electromagnetic scattering by arbitrarily shaped inhomogeneous dielectric bodies," *IEEE Trans. Antennas and Propagation*, vol. AP-32, no. 1, pp. 77-85, January 1984.
3. Liu Yaxun, S. Safavi-Naeini, and S. K. Chaudhuri, "Comparison of SIE-MoM and VIE-MoM for determination of complex resonant frequency of dielectric resonators", *IEEE-AP International Symposium, 2003*, IEEE, vol.1, pp. 641-644, June 2003.
4. T. Sarkar, S. M. Rao, and A. R. Djordjević, "Electromagnetic scattering and radiation from finite microstrip structures", *IEEE Trans. Microwave Theory and Techniques*, vol. 38, pp. 1568-1575, Nov. 1990.
5. N. A. Ozdemir and J. F. Lee, "Single level dual rank SVD algorithm for volume integral equations of electromagnetic scattering," in *Antennas and Propagation Society, 2003 IEEE International Symposium*, vol. 2, pp. 302 - 305, June 2003.
6. M. L. Barton and Z. J. Cendes, "New vector finite elements for three dimensional magnetic field computation", *J. Appl. Phys.,* vol. 61, No 8, pp. 3919-3921, 1987.
7. A. Bossavit, "Whitney forms: a class of finite elements for three dimensional computations in electromagnetism", *IEE Proceedings*, vol. 135, Pt. A, No 8, pp. 493-499, Nov. 1988.
8. Jin Fa Lee and R. Mittra, "A note on the application of edge elements for modeling three-dimensional inhomogeneously-filled cavities," *IEEE Trans. Microwave Theory and Techniques*, vol. MTT-40, pp. 1767-1773, Sept. 1992.
9. J. B. Manges and Z. J. Cendes, "A generalized tree-cotree gauge for magnetic field computation," *IEEE Trans. on Magnetics*, vol. 31, pp. 1342-1347, May 1995.
10. I. Tičar, O. Bíró, and K. Preis, "Vector potential expanded by edge basis functions associated with loops on finite-element facets," *IEEE Trans. on Magnetics*, vol. 38, pp. 437-440, March 2002.

11. S. A. de Carvalho and L. de Souza Mendes, "Scattering of EM waves by inhomogeneous dielectrics with the use of the method of moments and the 3-D solenoidal basis functions", *Microwave and Optical Technology Letters,* vol. 23, No. 1, pp. 42-46, Oct. 1999.
12. C. D. Meyer, *Matrix Analysis and Applied Linear Algebra*, SIAM, Philadelphia, PA, 2000.
13. B. J. Rubin, "Divergence-free basis for representing polarization current in finite-size dielectric regions," *IEEE Trans. Antennas and Propagation*, vol. 41, no. 3, pp. 269-277, March 1993.
14. Y. Saad, *Iterative Methods for Sparse Linear Systems*, Yousef Saad, 2000, p. 245.
15. A. W. Glisson, D. Kajfez, and J. James, "Evaluation of modes in dielectric resonators using a surface integral equation formulation," *IEEE Trans. Microwave Theory and Techniques*, vol. MTT-31, no. 12, pp. 1023-1029, Dec. 1983.
16. D. Kajfez and A. A. Kishk, "Dielectric resonator antenna – possible candidate for adaptive antenna arrays," Tutorial on *Dielectric Resonator Antenna*; online http://www.ee.olemiss.edu/darko/dra-pcfaaa.pdf
17. Intel Math Kernel Library Reference Manual. 2004. Online: http://www.intel.com/software/products/mkl/docs/mklman.pdf.
18. D. H. Staelin, A. W. Morgenthaler, and Jin A. Kong, *Electromagnetic Waves*, Prentice Hall, Upper Saddle River, NJ, 1990.
19. D. R. Wilton, S. M. Rao, A. W. Glisson, D. H. Schaubert, O. M. Al-Bundak, and C. M. Butler, "Potential integrals for uniform and linear source distribution on polygonal and polyhedral domains," *IEEE Trans. Antennas and Propagation*, vol. AP-32, no. 3, pp. 276-281, March 1984.
20. R. Cools, "An Encyclopedia of Cubature Formulas," *J. Complexity*, vol. 19, 445-453, 2003. Available onl.: http://www.cs.kuleuven.ac.be/~nines/research/ecf/ecf.html

21. S. Kulkarni and S. Makarov, "The effect of integration accuracy on the MoM VIE solution for dielectric resonators," *2005 IEEE Antennas and Propagation Int. Sym.*, Washington, DC, July 3-8, 2005.
22. S. Kulkarni and S. Makarov, "The effect of numerical integration on MoM VIE solution for some isolated dielectric resonators," *2005 ACES/IEEE Int. Conf. Wireless Communications Applied Electromagnetics*, Honolulu, 3-7 April 2005.